Metabolic engineering of Escherichia coli for 4-nitrophenylalanine production via the 4-aminophenylalanine synthetic pathway

Mori, Ayana ; Hirata, Yuuki ; Kishida, Mayumi ; Nonaka, Daisuke ; Kondo, Akihiko ; Mori, Yutaro ; Noda, Shuhei ; Tanaka, Tsutomu

(Citation)
Metabolic Engineering,91:171-180

(Issue Date)
2025-09

(Resource Type)
journal article

(Version)
Version of Record

Metabolic Engineering 91 (2025) 171–180

Contents lists available at ScienceDirect

Metabolic Engineering

journal homepage: www.elsevier.com/locate/meteng

Metabolic engineering of *Escherichia coli* for 4-nitrophenylalanine production via the 4-aminophenylalanine synthetic pathway

Ayana Mori [a], Yuuki Hirata [a], Mayumi Kishida [a], Daisuke Nonaka [a], Akihiko Kondo [b], Yutaro Mori [a], Shuhei Noda [b,c,*], Tsutomu Tanaka [a,**]

[a] Department of Chemical Science and Engineering, Graduate School of Engineering, Kobe University, 1-1 Rokkodai-cho, Nada-ku, Kobe, Hyogo, 657-8501, Japan
[b] Graduate School of Science, Technology and Innovation, Kobe University, 1-1 Rokkodai-cho, Nada-ku, Kobe, Hyogo, 657-8501, Japan
[c] PRESTO, Japan Science and Technology Agency (JST), Kawaguchi, 332-0012, Saitama, Japan

ARTICLE INFO

Keywords:
4-Nitrophenylalanine
4-Aminophenylalanine
Nitro compounds
Microbial production

ABSTRACT

The non-natural amino acid 4-nitrophenylalanine is a crucial pharmaceutical ingredient and has extensive utility in protein engineering. Here, we demonstrated the production of 4-nitrophenylalanine by *Escherichia coli* with AurF, 4-aminobenzoate *N*-oxygenase from *Streptomyces thioluteus*. Firstly, eight distinct gene combinations, encompassing four variants of *papA* and two of *papBC*, were evaluated to optimize the production of 4-aminophenylalanine, a precursor of 4-nitrophenylalanine. The strain co-expressing both *pabAB* from *E. coli* and *papBC* from *Streptomyces venezuelae* attained the highest 4-aminophenylalanine production. In a fed-batch fermenter cultivation, 4-aminophenylalanine production of 22.5 g/L was achieved. To produce 4-nitrophenylalanine from glucose, we constructed strains co-expressing AurF alongside the genes responsible for 4-aminophenylalanine synthesis. The subsequent optimization of the plasmid copy numbers carrying each gene set resulted in an increase in the 4-nitrophenylalanine production titer. Transcription analysis revealed that the expression level of the 4-aminophenylalanine biosynthetic genes markedly contributed to 4-nitrophenylalanine production. After optimizing batch fermentation conditions, the titer of 4-nitrophenylalanine increased to 2.22 g/L. Overall, these results provide the basis for industrial microbial production of 4-nitrophenylalanine, contributing to the advancement of biotechnological methodologies for generating non-natural amino acids with specific functionalities.

1. Introduction

Nitroaromatic compounds constitute an important and extensively synthesized category within the industrial sector, serving multifaceted purposes. They find applications as explosives (e.g., picric acid, trinitrotoluene; TNT), pharmaceuticals (e.g., antibiotic chloramphenicol), dyes (e.g., 1-[(E)-(4-Nitrophenyl)diazinyl] naphthalen-2-ol; para red), and pesticides (e.g., o, o-Diethyl o-(4-nitrophenyl) phosphorothioate; parathion). Leveraging the potent electronegativity of the nitro group, these compounds induce π-electron delocalization within the aromatic ring. This property enhances their reactivity with nucleophiles, broadening the scope of compound transformations and accentuating their value as materials. Nitroaromatic compounds are commonly synthesized through aromatic ring nitration using nitronium ions derived from sulfuric and nitric acids (Siddharth et al., 2021). However, this method demands rigorous conditions, necessitating precise control to avert explosive outcomes. Furthermore, excessive acid usage and its subsequent disposal pose environmental problems. Enzymatic and microbial production methods have emerged as promising alternatives to conventional synthesis, as they operate under milder conditions, showcasing heightened specificity and environmental compatibility.

To date, two classes of enzymes that facilitate nitrocompound synthesis have been identified in nature (Nóbile et al., 2021). First, *N*-oxygenases catalyze nitrogroup synthesis by oxidizing the amino groups. Examples include AurF from *Streptomyces thioluteus*, which is associated with antibiotic aureothin biosynthesis (He and Hertweck, 2004), CmlI from *Streptomyces venezuelae*, which contributes to chloramphenicol biosynthesis (Lu et al., 2012), and PrnD from *Pseudomonas*

* Corresponding author. PRESTO, Japan Science and Technology Agency (JST), Kawaguchi 332-0012, Saitama, Japan
** Corresponding author. Department of Chemical Science and Engineering, Graduate School of Engineering, Kobe University, 1-1 Rokkodai-cho, Nada-ku, Kobe, Hyogo 657-8501, Japan
E-mail addresses: shuhei.noda@opal.kobe-u.ac.jp (S. Noda), tanaka@kitty.kobe-u.ac.jp (T. Tanaka).

https://doi.org/10.1016/j.ymben.2025.04.006
Received 18 September 2024; Received in revised form 17 March 2025; Accepted 26 April 2025
Available online 27 April 2025

fluorescens, which participates in pyrrolnitrin biosynthesis (J. K. Lee et al., 2006). Second, a subset of cytochrome P450 enzymes facilitates the direct nitration of benzene rings. Notable examples include TxtE from *Streptomyces scabies*, which is involved in phytotoxin thaxtomin biosynthesis (Barry et al., 2012), and RufO from *Streptomyces atratus*, which participates in rufomycin biosynthesis (Tomita et al., 2017). However, enzymes dedicated to nitrocompound synthesis remain relatively scarce compared with those involved in the synthesis of other compound classes (e.g., amino, carboxy, and hydroxy compounds), with only approximately 200 nitrocompounds identified in nature to date (Butler et al., 2023). This scarcity partly accounts for the limited advancement in enzymatic nitration synthesis despite its advantages over traditional synthetic methodologies.

Among the identified nitrocompounds, 4-nitrophenylalanine (NPhe), a non-natural amino acid and an analog of the essential amino acid phenylalanine. NPhe holds particular significance due to its nitrogroup-induced electron-withdrawing potential. NPhe markedly contributes to the synthesis of biochemical reagents and medicinal intermediates and serves as an intermediate in the production of zolmitriptan (X. Liu et al., 2020), a compound employed in migraine treatments. NPhe finds applications in protein engineering through genetic code expansion, conferring functionality to proteins, such as enhanced immunogenicity (Gauba et al., 2011), and functioning as a distance probe (Tsao et al., 2006).

Butler et al. (2023) first investigated the microbial production of NPhe by utilizing 4-aminophenylalanine (APhe) as a precursor for NPhe production in *Escherichia coli*. By introducing *S. venezuelae*-derived *papABC* genes associated with APhe production and *Pseudomonas* sp.-derived nonheme diiron *N*-monooxygenase NO16, they successfully produced 820 μM of NPhe. This pioneering work exemplifies the potential of microbial synthesis for the sustainable production of valuable chemical compounds, with considerable room for improvement in the NPhe titer.

APhe, a precursor of NPhe, is used for a variety of applications as well as NPhe. APhe is a crucial material for synthesizing high-performance polymers (Hirayama et al., 2020) and a precursor for polyamide building blocks, such as *p*-aminohydroxycinnamic acid (Kawasaki et al., 2018; Tateyama et al., 2016). In pharmaceutical applications, APhe serves as a starting material for synthesizing the anticancer drug melphalan (Jobdevairakkam and Velladurai, 2009). In addition, an attempt has been made to integrate APhe into the structure of the jadomycin antibiotic to add other functionalities (Martinez-Farina et al., 2015). In nature, APhe occurs as an intermediate of chloramphenicol and pristinamycin by *S. venezuelae* and *S. pristinaespiralis*, respectively (Blanc et al., 1997; He et al., 2001). Furthermore, a gene cluster for APhe synthesis was discovered in *P. fluorescence* (Masuo et al., 2016). Three genes, *papA*, *papB*, and *papC,* play a central role in APhe synthesis. The process begins with PapA, 4-amino-4-deoxychorismate synthase, replacing the hydroxy group with an amino group of chorismate, which is an intermediate of the shikimate pathway. PapB (4-amino-4-deoxychorismate mutase) and PapC (4-amino-4--deoxyprehenate dehydrogenase) then convert 4-amino-4-deoxychorismate to 4-aminophenylpyruvate, which is a substrate for aminotransferases, and is converted to APhe. Aminotransferases TyrB and AspC from *E. coli* are known to catalyze this conversion (Hayashi et al., 1993; Onuffer et al., 1995). Masuo et al. demonstrated 4.4 g/L APhe production from glucose in fed-batch cultivation using recombinant *E. coli* with *papABC* from *P. fluorescence* (Masuo et al., 2016). An *E. coli* strain introduced with *pabAB* from *Corynebacterium glutamicum* and *papB* and *papC* from *S. venezuelae* produced 16.7 g/L APhe from glycerol in fed-batch fermenter cultivation (Mohammadi Nargesi et al., 2018).

In this study, we initially sought to identify an *N*-oxygenase capable of catalyzing NPhe biosynthesis, leading to the selection of AurF from *S. thioluteus* as a viable candidate. Subsequently, we systematically evaluated eight gene combinations for APhe synthesis. Notably, the strain incorporating *pabAB* from *E. coli* and *papBC* from *S. venezuelae* exhibited the highest APhe titer in the test tube culture (2.52 g/L). The integration of the full pathway context and optimization of plasmid copy numbers enabled *E. coli* to synthesize 843 mg/L of NPhe from 20 g/L glucose. Furthermore, cultivations using jar fermenters increased the production titers of NPhe and APhe up to 2.22 and 22.5 g/L, respectively.

2. Materials and Methods

2.1. Strain and plasmid construction

E. coli NovaBlue competent cells (Novagen, Cambridge, MA, USA) were used for gene cloning. PCR was performed using KOD-Multi and Epi-DNA polymerase (Toyobo, Osaka, Japan) or KOD FX Neo (Toyobo, Osaka, Japan). *E. coli* BL21 Star™ (DE3) competent cells (Thermo Fisher Scientific, Massachusetts, USA) were used for protein expression for enzyme purification. Tables S1 and S2 contain the strains and primer pairs used. Each gene was assembled with its respective plasmids using the NEBuilder HiFi DNA Assembly Master Mix (New England Biolabs, Ipswich, MA, USA).

pNE12-Ptrc was constructed as follows: The *trc* promoter region was amplified via PCR using pTrcHisB as the template and trc_to_pze_fw and trc_to_pze_rv as the primer pair. The plasmid gene fragment was also amplified via PCR using pZE12-MCS as the template and inv_pze_fw and inv_pze_rv as the primer pair. The amplified fragments were conjugated together, and the plasmid obtained was named pNE12-Ptrc. pNA23-Ptrc and pNCD-Ptrc were constructed similarly.

pSAK-PabAB was constructed as follows. The PabABC gene fragment was amplified via PCR using pZE12PabABC as the template and lac_pababc_fw and lac_pababc_rv as the primer pair. The amplified fragment was introduced into the *Kpn*I site of pSAK, and the plasmid obtained was named pSAK-PabABC. The pSAK-PabAB fragment was amplified via PCR using pSAK-PabABC as the template and inv_psak-ab_fw and inv_psak-ab_rv as the primer pair. The amplified fragment was self-ligated, and the plasmid obtained was named pSAK-PabAB.

pNE-Ptrc-EcpabAB-PfpapBC was constructed as follows. The pNE-Ptrc gene fragment was amplified via PCR using pNE12-Ptrc as the template and inv_12_trc_fw and inv_12_trc_rv as the primer pair. The EcpabAB gene fragment was amplified via PCR using pSAK-PabAB as the template and ecpabab_to_trc_fw and ecpabab_rv as the primer pair. PfpapBC gene fragment was amplified via PCR using the PfpapBC synthetic gene as template and rbs_pfpapbc_ecpabab_fw and pfpapbc_-to_trc_rv as the primer pair. The amplified fragments were conjugated together, and the plasmids obtained were named pNE-Ptrc-EcpabAB-PfpapBC. The following plasmids were constructed similarly: pNE-Ptrc-EcpabAB-SvpapBC, pNE-Ptrc-PfpapA-PfpapBC, pNE-Ptrc-PfpapA-SvpapBC, pNE-Ptrc-SvpapA-PfpapBC, pNE-Ptrc-SvpapA-SvpapBC, pNE-Ptrc-CgpabAB-PfpapBC and pNE-Ptrc-CgpabAB-SvpapBC.

pSAK-Ptrc-EcpabAB-PfpapBC was constructed as follows. The pSAK-Ptrc gene fragment was amplified via PCR using pSAK-Ptrc as the template and inv_trc_fw and inv_trc_rv as the primer pair. The EcpabAB-PfpapBC gene fragment was also amplified via PCR using pNE-Ptrc-EcpabAB-PfpapBC as the template and ecpabab_to_trc_fw and pfpapbc_trc_rv as the primer pair. The amplified fragments were conjugated together, and the plasmids obtained were named pSAK-Ptrc-EcpabAB-PfpapBC. pNA23-Ptrc-EcpabAB-PfpapBC, pNCD-Ptrc-EcpabAB-PfpapBC, pSAK-Ptrc-EcpabAB-SvpapBC, pNA23-Ptrc-EcpabAB-SvpapBC, and pNCD-Ptrc-EcpabAB-SvpapBC were constructed similarly.

pZE12-obiL was constructed as follows. A codon-optimized foreign gene fragment of *obiL* from *Pseudomonas fluorescens* strain ATCC39502 was synthesized by an Artificial Gene Synthesis service (Twist Bioscience, San Francisco, CA, USA). The gene fragment encoding *obiL* amplified by PCR using the primer pair pZ-obiL_fw and pZ-obiL_rv. The amplified fragments were cloned between the *Kpn*I/*Hind*III site of

pZE12MCS. pSAK-obiL was constructed similarly. pZE12-NO16 and pSAK-NO16 was constructed similarly with a codon-optimized foreign gene fragment encoding NO16 from *Pseudomonas* sp. EMN2 synthesized by an Artificial Gene Synthesis service (Twist Bioscience, San Francisco, CA, USA).

pETDuet-*aurF* was constructed as follows. The gene encoding AurF was amplified by PCR using the primer pair pET-aurF_Fw and pET-aurF_Rv. The amplified fragments were cloned between the *EcoR*I/*Hin*dIII site of pETDuet-1. pRSFDuet-obiL and pRSFDuet-NO16 were constructed similarly with pRSFDuet-1.

The disruption of *pykA* and *pykF* was performed using the CRISPR-Cas9-plasmid system (Jiang et al., 2015) with pTΔ*pykA* and pTΔ*pykF*.

2.2. Medium

LB medium was used for preculture and culture for genetic manipulation. The LB medium comprised 10 g/L tryptone, 5 g/L yeast extract, and 5 g/L NaCl. The M9Y medium was used for APhe and NPhe production. The M9Y medium contained 20 g/L glucose, 5 g/L yeast extract, 6 g/L Na_2HPO_4, 3 g/L KH_2PO_4, 2 g/L NH_4Cl, 0.5 g/L NaCl, 1 mM $MgSO_4{\cdot}7H_2O$, 0.1 mM $CaCl_2{\cdot}2H_2O$, 0.1 mM $FeSO_4{\cdot}7H_2O$, 10 mg/L thiamine hydrochloride, and 0.1 mM IPTG. 100 mg/L ampicillin, 100 mg/L spectinomycin, 50 mg/L kanamycin, and 30 mg/L chloramphenicol were added, if needed. L-phenylalanine (100 mg/L), L-tyrosine (40 mg/L), L-tryptophan (40 mg/L), and sodium pyruvate (1.1 g/L) were added during CFT5 and PN-5 strain cultivation.

2.3. Cultivation conditions

E. coli colonies from the LB plates were inoculated into test tubes containing 5 mL of LB medium and incubated overnight at 37 °C and 220 rpm. The preculture solution was then inoculated into test tubes containing 5 mL of M9Y medium to initial OD_{600} = 0.05 and incubated at 37 °C and 220 rpm for 48 h (Fig. 1B, Fig. S1) or 72 h (Figs. 1C and 6, Fig. S3) or 96 h (Figs. 2, 4 and 5). For analyses of bacterial cell growth and metabolites, 400 μL of the solution was collected and centrifuged at 10,000 rpm for 10 min. The supernatant was analyzed by high-performance liquid chromatography (HPLC).

2.4. Fermentation in a bioreactor

DO-stat fed-batch and batch fermentations were performed in a 1-L

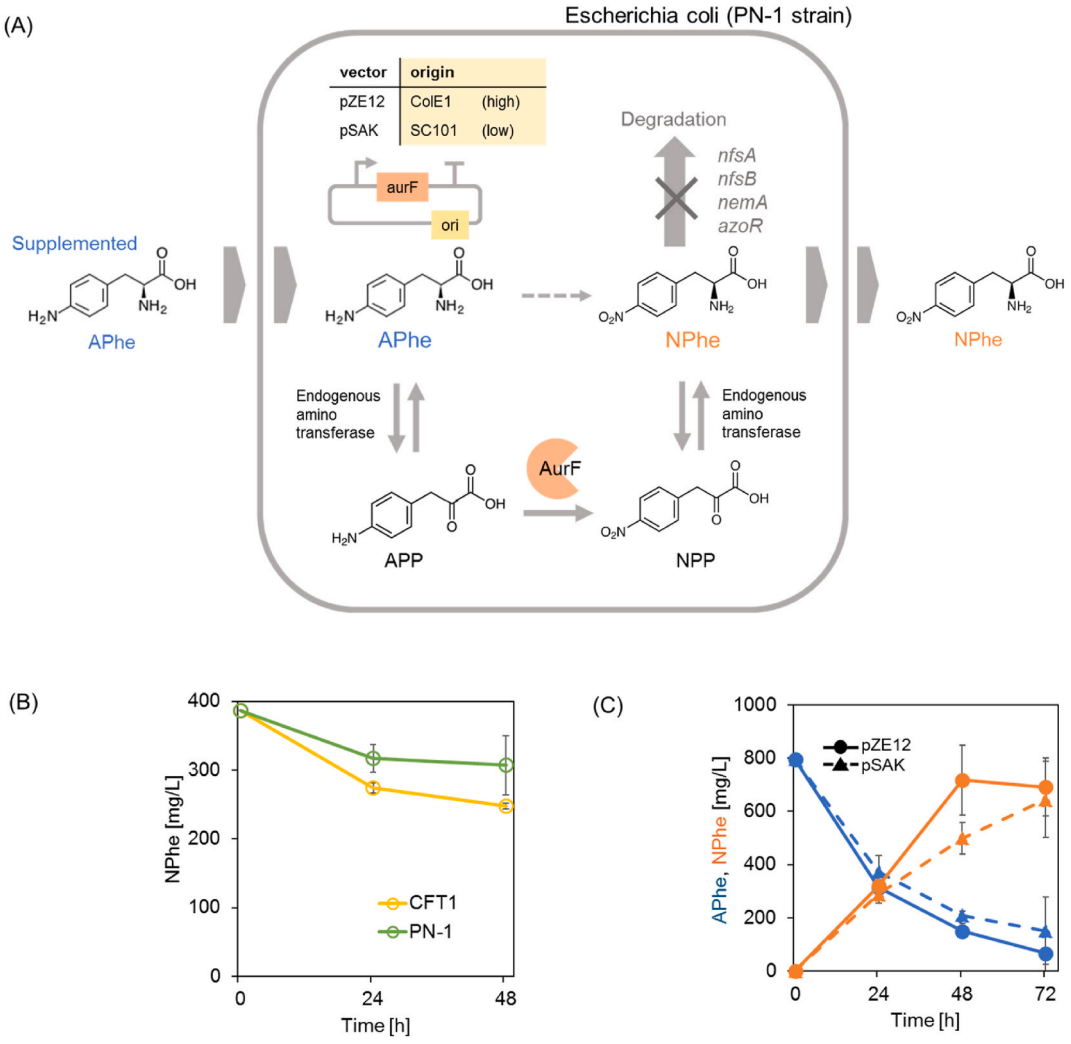

Fig. 1. (A) Schematic illustration of NPhe production from APhe. APhe, 4-aminophenylalanine; NPhe, 4-nitrophenylalanine; APP, 4-aminophenylpyruvate; NPP, 4-nitrophenylpyruvate; AurF; *p*-aminobenzoate *N*-oxygenase. **(B)** Evaluation of NPhe degradation. The NPhe concentrations during the cultivation of CFT1 (yellow) and PN-1 (green) are shown. **(C)** Time courses of NPhe production from APhe as a precursor. APhe (795 mg/L) was initially added to the medium during the cultivation of PN-1a (circles and solid lines) and PN-1A (triangles and dashed lines). APhe and NPhe concentrations are shown in blue and orange, respectively. The data are shown as the means of three independent experiments with standard deviations. (For interpretation of the references to colour in this figure legend, the reader is referred to the Web version of this article.)

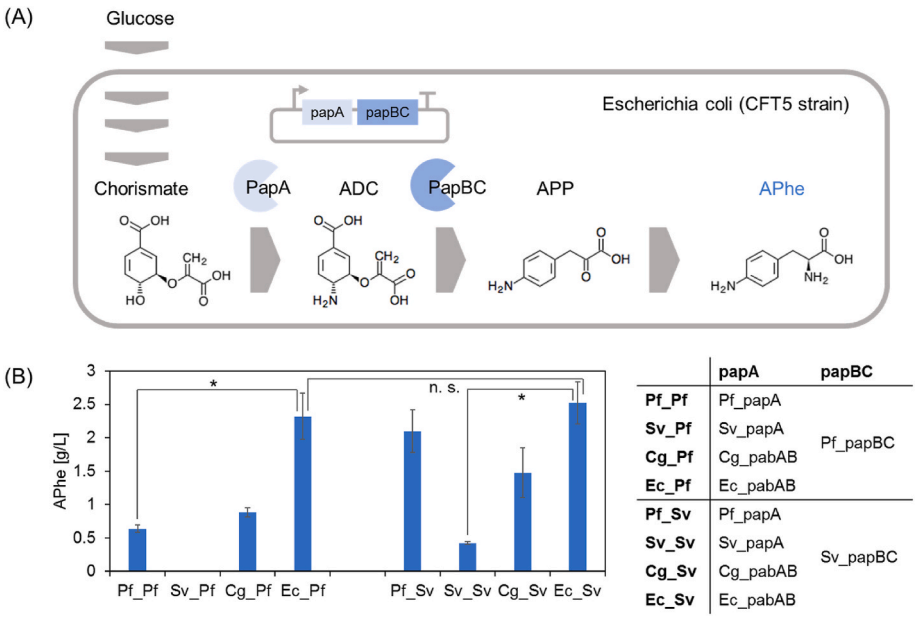

Fig. 2. APhe production from gl**ucose. (A)** Metabolic pathway for APhe production from glucose. ADC, 4-amino-4-deoxychorismate; APP, 4-aminophenylpyruvate; APhe, 4-aminophenylalanine; PapA, 4-amino-4-deoxychorismate synthase; PapB, 4-amino-4-deoxychorismate mutase; PapC, 4-amino-4-deoxyprehenate dehydrogenase. (B) Evaluation of gene combinations on APhe production after 96 h cultivation. The data are shown as the means of three independent experiments with standard deviations. Asterisks indicate significant difference: *$p < 0.05$.

bioreactor (ABLE & Biott, Tokyo, Japan) with a working volume of 600 mL. The medium comprised 20 g/L glucose, 5 g/L yeast extract, 6 g/L Na_2HPO_4, 3 g/L KH_2PO_4, 2 g/L $(NH_4)_2SO_4$, 0.5 g/L NaCl, 1.1 g/L (for APhe) or 5.5 g/L (for NPhe) pyruvate sodium, 100 mg/L L-phenylalanine, 100 mg/L L-tyrosine, 100 mg/L L-tryptophan, 1 mM $MgSO_4{\cdot}7H_2O$, 0.1 mM $CaCl_2{\cdot}2H_2O$, 0.01 mM $FeSO_4{\cdot}7H_2O$, 10 mg/L thiamine hydrochloride, and 0.1 mM IPTG. In addition, 200 mg/L ampicillin and 30 mg/L chloramphenicol were added if needed. The strains were inoculated into 200-mL shake flasks containing 50 mL of the medium and cultivated overnight at 37 °C and 220 rpm. The preculture solution was added to a jar fermenter containing the medium with an initial OD_{600} of 0.05 (for APhe) or 0.3 (for NPhe). Next, 110 g/L pyruvate sodium was added at a rate of 10 mL/day until DO-stat feeding started, and the pH was maintained at 7.0 with aqueous ammonia and sulfuric acid. The flow rate of air for fermentation was maintained at 1.2 L/min (for APhe) or 0.4 L/min (for NPhe). The dissolved oxygen (DO) level was maintained at 30 % by automatically controlling the agitation speed. The feed solution for APhe production contained 480 g/L glucose, 6.4 g/L $MgSO_4{\cdot}7H_2O$, 0.08 mM $CaCl_2{\cdot}2H_2O$, 0.008 mM $FeSO_4{\cdot}7H_2O$, 8 mg/L thiamine hydrochloride, 0.8 mM IPTG, 80 mg/L L-phenylalanine, 80 mg/L L-tyrosine, 80 mg/L L-tryptophan, and 200 mg/L ampicillin.

2.5. Analytical methods

Bacterial cell growth was evaluated by measuring the optical density at 600 nm using a UVmini-1240 spectrophotometer (Shimadzu Corporation, Kyoto, Japan). For APhe and 4-aminophenylpyruvate (APP) analysis, HPLC (Shimadzu Corporation) equipped with a PBr column (5 μm, 4.6 mm I.D. × 250 mm L; Nacalai Tesque, Kyoto, Japan) was used. HPLC profiles were obtained using a 254-nm UV–VIS detector. A two-component system was used, and the mobile phase was (A) 20 mM potassium phosphate buffer (pH7) and (B) methanol. The gradient started with a 98:2 mixture of A and B and shifted to a 50:50 mixture gradually from 7 min, with this ratio retained from 10 to 12 min. The mixture was then returned to a 98:2 ratio at 15 min. The mobile phase flow rate was 1.0 mL/min, and the column remained at 40 °C. For 4-nitrophenylpyruvate (NPP) analysis, HPLC (Shimadzu Corporation) equipped with a PBr column (5 μm, 4.6 mm I.D. × 250 mm L; Nacalai Tesque, Kyoto, Japan) was used. HPLC profiles were obtained using a 254-nm UV–VIS detector. The mobile phase was a 1:1 mixture of 20 mM potassium phosphate buffer (pH7) and methanol. For NPhe analysis, HPLC (Shimadzu Corporation) equipped with an MSII column (5 μm, 4.6 mm I.D. × 250 mm L; Nacalai Tesque) was used. HPLC profiles were obtained using a 254-nm UV–VIS detector. A two-component system was used, and the mobile phase was (A) 0.2 % phosphate buffer and (B) methanol. The gradient started with a 70:30 mixture of A and B and shifted to a 50:50 mixture gradually from 4 min, with this ratio retained from 6 to 14 min. The mixture was then returned to a 70:30 ratio at 16 min. The mobile phase flow rate was 1.0 mL/min, and the column remained at 40 °C. For glucose analysis, prominence HPLC (Shimadzu Corporation) equipped with a Shodex SUGAR KS-801 column (6 μm, 8.0 mm I.D. × 300 mm L; Shodex) was used. The mobile phase was water, and HPLC profiles were obtained using a refractive index detector. The flow rate was 0.8 mL/min, and the column was maintained at 50 °C.

2.6. Quantification of mRNA transcription levels using real-time PCR

The transcriptional expression of pabB and aurF in each strain was quantified using real-time PCR. Total RNA was isolated from individual cultures using a NucleoSpin RNA column (Takara Bio, Shiga, Japan) following the manufacturer's protocol. Reverse transcription reactions and quantitative real-time PCR were performed using a LightCycler 96 system (Roche Diagnostics) and an RNA-direct SYBR Green real-time PCR master mix (TOYOBO, Osaka, Japan). Table S2 contains the primer pairs used. The normalized transcriptional level of each mRNA was calculated using the relative quantification method, with the 16 S rRNA gene serving as the housekeeping gene.

2.7. Expression, purification and activity assay of AurF, ObiL and NO16

AurF, ObiL and NO16 were expressed by *E. coli* BL21 star (DE3) strain harboring pETDuet-aurF, pRSFDuet-obiL and pRSFDuet-NO16, respectively. Protein purification was carried out using TALON® Metal Affinity Resin (Takara Bio, Shiga, Japan) according to manufactures' procedure. Enzymatic reactions were performed in a total volume of 30 μL, containing 10 μM enzyme, 2.5 mM NADH, 0.25 mM PMS, 10

μM $FeSO_4$, 25 mM NaCl and 25 mM Na_2HPO_4 (pH 7). Substrate concentrations ranged from 0.03 to 2 mM APhe or APP. The reaction mixtures were incubated at 37 °C for 10 min (APhe) or 5min (APP) and subsequently quenched by adding 1 M HCl. The resulting products were analyzed using HPLC as described above.

3. Results and discussion

3.1. 4-Nitrophenylalanine production from 4-aminophenylalanine using AurF

In our previous study, we observed the proclivity of *E. coli* to degrade *p*-nitrobenzoate (Mori et al., 2023). Although the pathway for degrading nitrocompounds remains partially elucidated, we constructed a PN-1 strain featuring the disruption of four genes: nitroreductases encoded by *nfsA* and *nfsB*, N-ethylmaleimide reductase encoded by *nemA*, and azoreductase encoded by *azoR* (Mori et al., 2023) (Fig. 1A). To evaluate NPhe degradation, strain PN-1 and its parental strain CFT1 were used. The CFT1 strain exhibited 150 mg/L degradation of NPhe within 48 h (Fig. 1B). In contrast, PN-1 demonstrated a more subdued degradation, reaching only 70 mg/L degradation of NPhe (Fig. 1B). Furthermore, an NPhe degradation experiment was conducted using CFT1Δ *nfsA*, CFT1Δ*nfsA*Δ*nfsB* and CFT1Δ*nfsA*Δ*nfsB*Δ*nemA*, to identify the predominant genes involved in NPhe degradation (Fig. S1). The results showed statistically significant differences between CFT1 and the strains CFT1Δ *nfsA*, CFT1Δ*nfsA*Δ*nfsB*Δ*nemA* and PN-1. Conversely, no significant differences were observed among CFT1Δ*nfsA*, CFT1Δ*nfsA*Δ*nfsB* and CFT1Δ*nfsA*Δ*nfsB*Δ*nemA*, suggesting that *nfsA* and *azoR* are the primay genes involved in NPhe degradation. Consequently, the PN-1 strain is suitable for NPhe production.

In the present study, we focused on the *N*-oxygenase AurF derived from *Streptomyces thioluteus*. Notably, AurF is classified as a nonheme diiron monooxygenase in the same group as ObiL and NO16, which are used for NPhe production (Butler et al., 2023). AurF can oxidize an amino group of *p*-aminobenzoate, an intermediate of the folate biosynthesis pathway, to synthesize *p*-nitrobenzoate (He and Hertweck, 2004). AurF can be used to synthesize other natural and/or non-natural nitroaromatic compounds due to its broad substrate specificity (Chanco et al., 2014). The analysis of AurF substrate specificity *in vitro* indicated that it does not recognize APhe as its substrate or produce NPhe (Chanco et al., 2014). However, we hypothesized that AurF might possess the capacity to oxidize 4-aminophenylpyruvate (APP), a metabolic intermediate that undergoes reversible conversion from APhe via endogenous aminotransferases (Fig. 1A).

To evaluate AurF's potential for NPhe biosynthesis, PN-1a and PN-1A strains carrying the *aurF* gene on high-copy vectors or low-copy vectors, respectively (Mori et al., 2023), were used. These strains were cultivated in M9Y medium supplemented with 0.8 g/L of APhe. Notably, both strains successfully converted APhe into NPhe (Fig. 1C), demonstrating AurF's catalytic competence in this pathway (Fig. 1A). After 48 h of cultivation, PN-1a produced 717 mg/L NPhe from 795 mg/L of APhe, corresponding to a molar conversion efficiency of 0.85 mol/mol (Fig. 1C). In contrast, PN-1A demonstrated an exhibited a lower NPhe titer of 499 mg/L, with a conversion efficiency of 0.59 mol/mol. These results suggest that AurF is a viable candidate for NPhe biosynthesis and that a high-copy vector enhances its catalytic efficiency.

3.2. Evaluation of gene combinations and fed-batch fermentation for 4-aminophenylalanine synthesis

We systematically assessed various combinations of PapA, PapB, and PapC for APhe synthesis. We selected PapABCs from the native APhe producing strains, *P. fluorescence* and *S. venezuelae*. Additionally, given that PapA shares functional similarity with PabAB in folate biosynthesis, we chose PabAB from *E. coli* and *C. glutamicum* as potential candidates. Thus, four distinct PapA variants and two PapBC types were examined. Each set of *papABC* genes was inserted into the pNE12-Ptrc vector, and the plasmids were introduced into the CFT5 strain, which was previously constructed for its proficiency in aromatic compound production (Noda et al., 2016) (Fig. 2A). Strains expressing Ec_PabAB and Pf_PapBC or Ec_PabAB and Sv_PapBC yielded APhe titers of 2.32 g/L and 2.52 g/L, respectively, after 96 h of cultivation, which was the highest titer (Fig. 2B). In contrast, the original combination, Pf_Pf (PapABC from *P. fluorescens*) and Sv_Sv (PapABC from *S. venezuelae*), produced only 0.64 g/L and 0.42 g/L, respectively. Interestingly, the strain expressing Pf_Sv (PapA from *P. fluorescens* and PapBC from *S. venezuelae*) exhibited a superior APhe yield of 2.10 g/L, surpassing that of the original gene combinations (Masuo et al., 2016; Mehl et al., 2003). Most previous studies on the microbial production of APhe have used a combination of Pf_PapA and Pf_PapBC or Sv_PapA and Sv_PapBC (Masuo et al., 2016; Mehl et al., 2003). In addition, a study using PabAB from *C. glutamicum* as PapA exists (Mohammadi Nargesi et al., 2018), but no previous studies have produced APhe using PabAB from *E. coli*. In this study, PabAB from *E. coli* proved more effective than PapA from other organisms, with no statistically significant difference observed between Ec_Pf and Ec_Sv (Fig. 2B). This suggests that PabAB from *E. coli* plays a crucial role in a high production titer of APhe. These findings demonstrate the significance of the combined action of *papABC* genes in optimizing APhe production.

DO-stat fed-batch fermentation was performed with the CFT5 strain harboring pNE12-Ptrc-EcpabAB-SvpapBC to increase APhe production (Fig. 3). The initial glucose concentration was 20 g/L. The pH was maintained at 7.0, and the DO level was maintained at 30 % by adjusting the agitation rate. The feeding solution containing 480 g/L glucose was automatically fed according to an increase in DO levels, indicating the complete consumption of glucose. After cultivation for 140 h, 22.5 g/L APhe was produced, achieving the highest APhe titer reported to date (Table 1). The yield of APhe in the bioreactor was approximately 0.37 g/g and that in the test tube culture was 0.13 g/g (Fig. 2B). In addition, the yield of APhe in the feeding phase exceeded that in the batch phase (0.39 vs. 0.30 g/g). These results suggest that DO-stat fed-batch fermentation is effective in improving APhe production. Although the cultivation time in this study was longer than that in other previous studies (Table 1), the APhe yield obtained in this study exceeded previously reported yields (0.17 g/g-glucose (Masuo et al., 2016), 0.13 g/g-glycerol (Mohammadi Nargesi et al., 2018)).

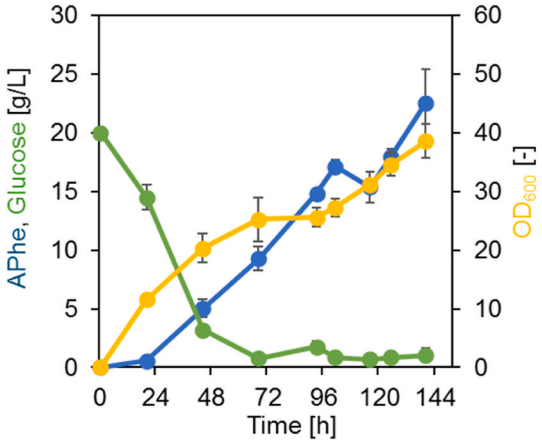

Fig. 3. DO-stat fed-batch fermentation in APhe production in a 1-L b**ioreactor.** APhe production, glucose concentration, and OD_{600} values are shown in blue, green, and yellow, respectively. The data represents the means of three independent experiments with standard deviations. (For interpretation of the references to colour in this figure legend, the reader is referred to the Web version of this article.)

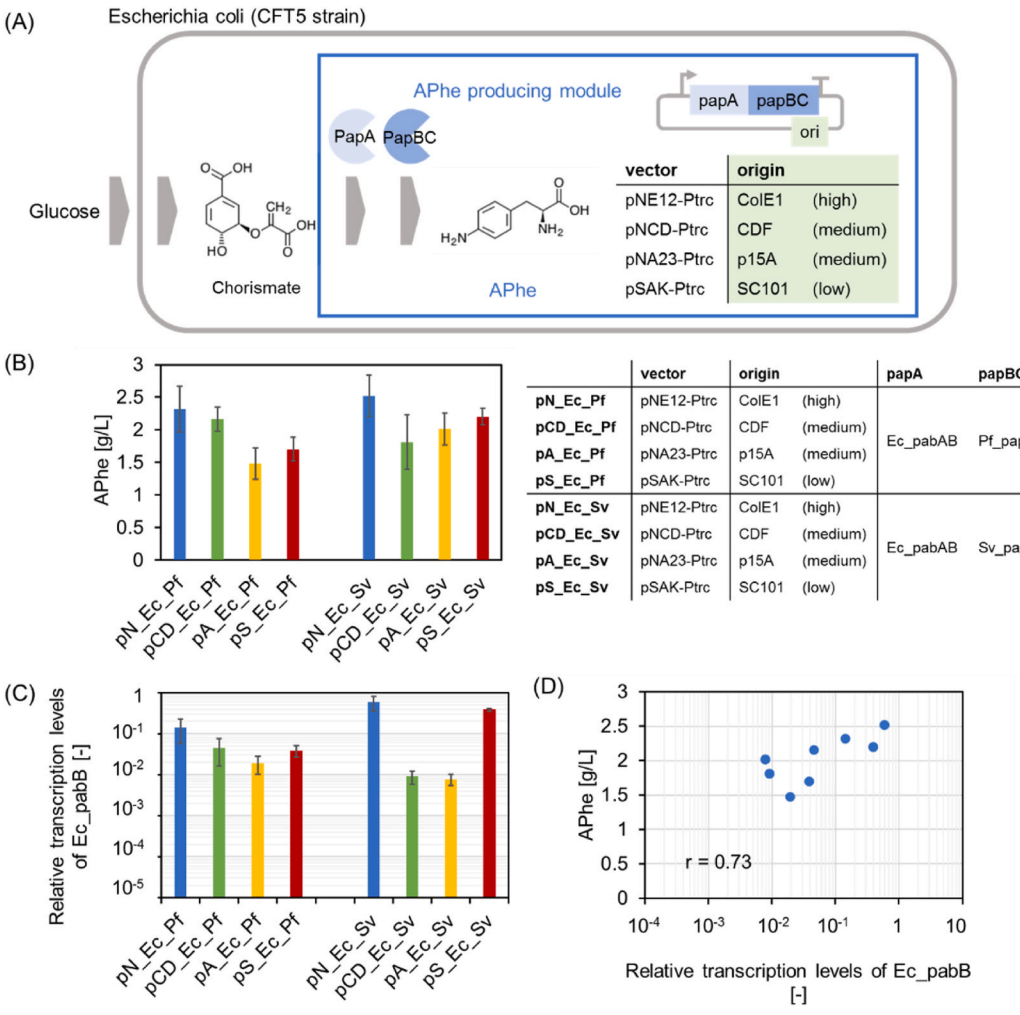

Fig. 4. Effect of plasmid copy numbers on APhe produ**ction. (A)** Schematic illustration of APhe production by tuning plasmid copy number. **(B)** APhe production by strains harboring plasmids that carry APhe synthetic genes and have distinct copy numbers. **(C)** Relative transcription levels of Ec_pabB. The data are shown as the means of three independent experiments with standard deviations. **(D)** Correlation between relative transcription levels of Ec_pabB and APhe production.

3.3. Engineering of 4-aminophenylalanine biosynthesis module for NPhe production by tuning plasmid copy number

Modular metabolic engineering is a widely used approach for optimizing metabolic pathways to enhance the productivity of target compounds. Expression levels of pathway modules are finely tuned using various regulatory tools, such as promoters, ribosome binding sites and codon usage. Plasmid copy number is one of the valuable tools for modular metabolic engineering. Lee and Trinh successfully engineered strains producing butyryl-CoA-derived designer esters by varying copy numbers of plasmids of each module (Jong-Won and Cong, 2022). Similarly, Yang et al. also achieved high tyrosol production through optimizing plasmid copy numbers (Haiquan et al., 2019). NPhe biosynthesis from glucose requires the introduction of both *aurF* and *papABC* into *E. coli* (Fig. 5A–D). Therefore, we opted modular metabolic engineering for NPhe production.

In the NPhe converting module, the high-copy vector pZE12-aurF significantly facilitated the conversion of APhe to NPhe (Fig. 1C). Similarly, in the APhe producing module, high APhe production from glucose was also attained using a high-copy vector. This emphasizes the importance of fine-tuning the expression levels of each module to optimize NPhe yield from glucose. Therefore, we engineered APhe producing module by tuning plasmid copy number and evaluated its effect on APhe production titers (Fig. 4A). Using a suite of plasmids with distinct origins of replication, we employed a high-copy number plasmid designated pNE12-Ptrc (ColE 1 origin), an intermediate copy number plasmid pNCD-Ptrc (CDF origin), pNA23-Ptrc (p15 A origin) for moderate expression levels, and a low-copy plasmid pSAK-Ptrc (SC101 origin) for the expression of two distinct PapABC enzyme pairs: Ec_PabAB/Pf_PapBC and Ec_PabAB/Sv_PapBC. As expected, we observed a pronounced decrease in APhe production concomitant with a reduction in the plasmid copy number (Fig. 4B). Intriguingly, despite the low-copy number of plasmid pSAK-Ptrc, the resultant APhe production (pS_Ec_Pf, 1.70 g/L; pS_Ec_Sv, 2.20 g/L) markedly exceeded that produced by medium-copy number plasmids (pA_Ec_Pf, 1.48 g/L; pA_Ec_Sv, 2.01 g/L, pCD_Ec_Sv, 1.81 g/L). To elucidate the underlying mechanisms contributing to this anomalous observation, we quantified the mRNA transcription levels of the Ec_pabB gene across the various strains by employing qRT-PCR (see Fig. 4C). We focused on the Ec_PabB transcription level because Ec_PabB can convert ammonia and chorismate to 4-amino-4-deoxychorismate on its own, whereas Ec_PabA cannot extract ammonia from glutamine without forming a complex with Ec_PabB. The correlation coefficient between the transcription levels of Ec_pabB and APhe production was 0.73 (Fig. 4D), indicating that high transcription levels of Ec_pabB lead to efficient APhe production. Notably, the transcriptional activity of the Ec_pabB gene in strains harboring the pSAK-Ptrc plasmid markedly exceeded that observed in strains with the pNCD-Ptrc and pNA23-Ptrc plasmids (Fig. 4C). This improved

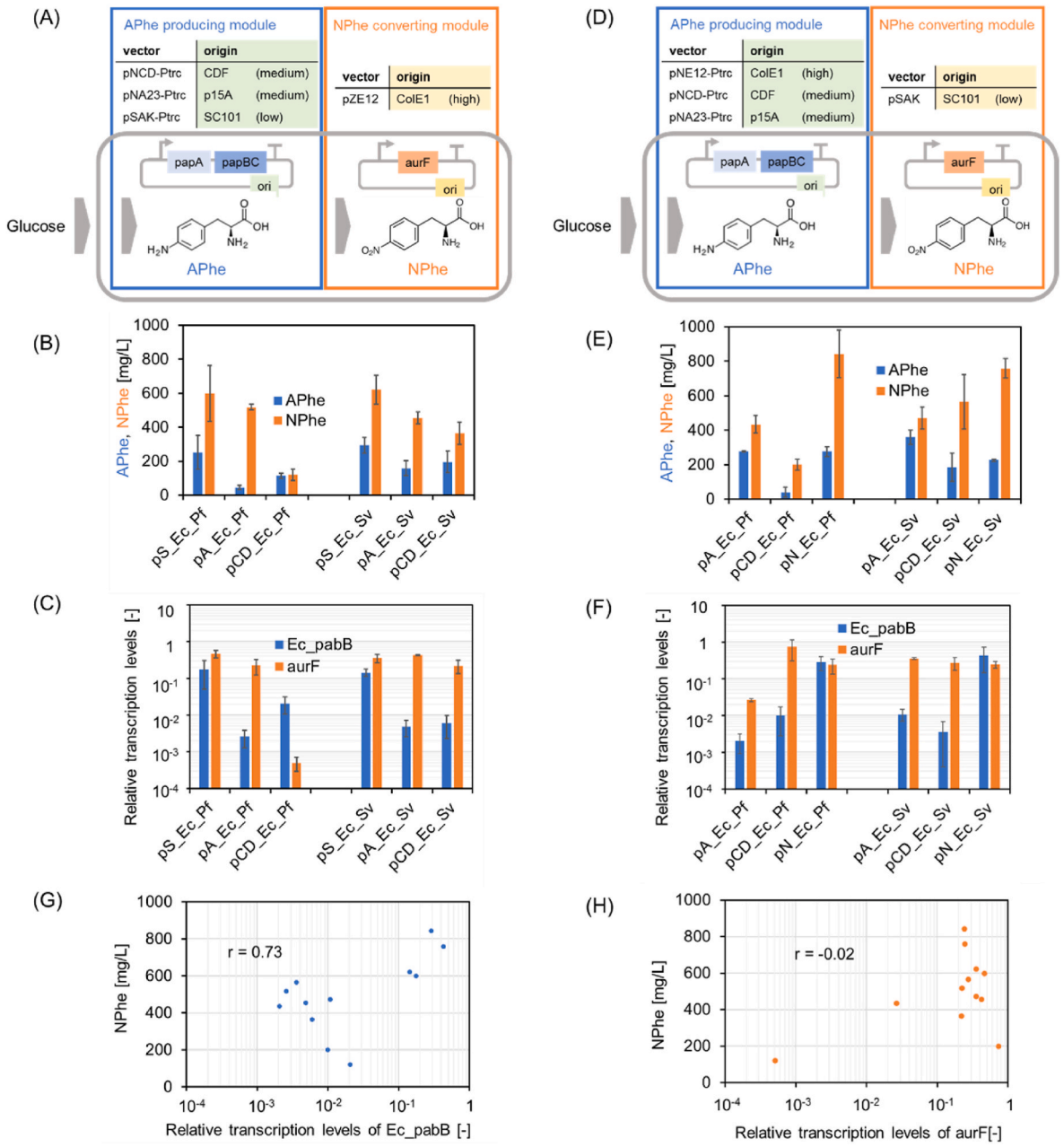

Fig. 5. NPhe production from glucose. **(A–C)** NPhe production by strains introduced with pZE12-aurF and low (pSAK-Ptrc) or medium (pNA23-Ptrc, pNCD-Ptrc) copy plasmids carrying APhe synthetic genes. **(D–F)** NPhe production by strains harboring pSAK-aurF and medium (pNA23-Ptrc, pNCD-Ptrc) or high (pNE12-Ptrc) copy plasmids carrying APhe synthetic genes. **(A)** and **(D)** show schematic illustrations. **(B)** and **(E)** show production titers of APhe and NPhe after 96 h cultivation. APhe and NPhe production titers are shown in blue and orange, respectively. **(C)** and **(F)** show relative transcription levels of Ec_pabB (blue) and aurF (orange) in the strains used in (B) and (E), respectively. The data are shown as the means of three independent experiments with standard deviations. **(G)** Correlation between the transcription levels of Ec_pabB and NPhe production performed with the strains used in (B) and (E). **(F)** Correlation between the transcription levels of aurF and NPhe production performed with the strains used in (B) and (E). (For interpretation of the references to colour in this figure legend, the reader is referred to the Web version of this article.)

transcriptional activity is believed to contribute to the enhanced APhe biosynthesis observed in low-copy number plasmid expression systems.

3.4. 4-Nitrophenylalanine production from glucose

In section 3.3, we optimized APhe producing module by adjusting the plasmid copy number. Based on this, we combined the APhe producing module with the NPhe converting module to produce NPhe from glucose (Fig. 5A–D). PN-5 strain (CFT5Δ*trpE*Δ*nfsA*Δ*nfsB*Δ*nemA*Δ*azoR*) was used as a parental strain. This strategic approach to vector combination and gene set expression aims to dissect the subtle interrelation between gene expression levels and metabolic pathway efficiency, thereby illuminating a pathway toward maximizing NPhe production from glucose through genetic and metabolic engineering in *E. coli*.

Fig. 5E shows the titers of NPhe and APhe when pSAK-aurF was used for NPhe converting module. After 96 h cultivation, pN_Ec_Pf yielded 843 mg/L of NPhe titer, followed by pN_Ec_Sv (758 mg/L) (Fig. 5E). When pZE12-aurF was used for NPhe converting module, pS_Ec_Pf and pS_Ec_Sv produced NPhe titers of 598 mg/L and 621 mg/L, respectively (Fig. 5B). Strains harboring pSAK-aurF were expected to have a lower conversion rate of APhe to NPhe and accumulate more APhe than those harboring pZE12-aurF (Fig. 1C), but the aurF expression vector had little

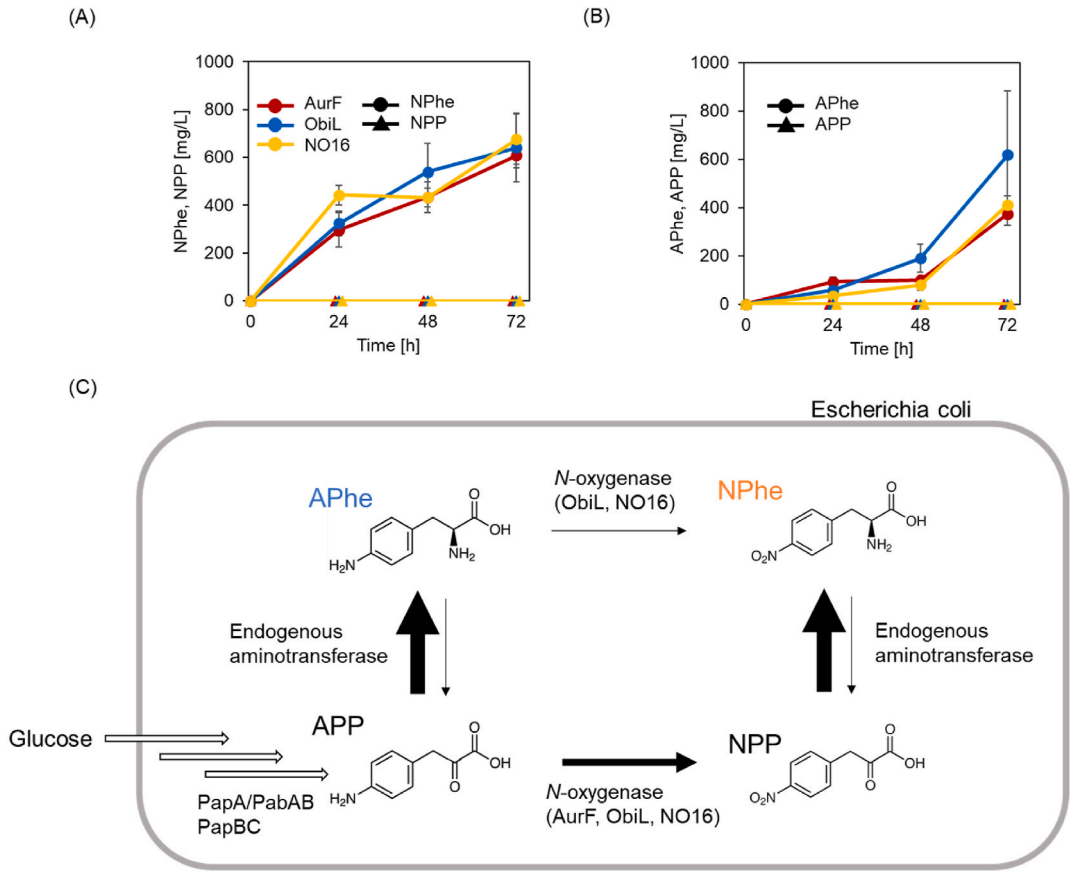

Fig. 6. (A, B) NPhe production from glucose in strains co-expressing EcpabAB-PfpapBC and AurF, ObiL, or NO16. The strains used were PN-5 carrying pNE12-Ptrc-EcpabAB-PfpapBC and pSAK-aurF (red), pSAK-obiL (blue), or pSAK-NO16 (yellow). (A) Time course of NPhe (circle) and NPP (triangle) production. (B) Time course of APhe (circle) and APP (triangle) accumulation. The data are shown as the means of three independent experiments with standard deviations. **(C)** Proposed metabolic flux model, illustrating the relative reaction rate magnitudes (black arrows). (For interpretation of the references to colour in this figure legend, the reader is referred to the Web version of this article.)

Table 1
APhe production by engineered *E. coli* strains.

Titer [g/L]	Yield [g/g-substrate]	Substrate	Condition	Time [h]	Overexpressed genes	Strains	Reference
22.5	0.37	glucose	Fed-batch	144	Ec_*pabAB* & Sv_*papBC*	ATCC31882Δ*ptsHI*::$P_{A1lacO-1}$-*glK-galP*Δ*pykF*Δ*pykA*Δ*pheA*Δ*tyrA*Δ*trpE*Δ*nfsA*Δ*nfsB*Δ*nemA*ΔΔ*azoR*	This study
16.78	0.13	glycerol	Fed-batch	77	Cg_*pabAB* & Sv_*papBC* & *aroFBL*	W3110Δ*pheA*Δ*tyrA*Δ*aroF*Δ*lac*::P_{tac}-*aroFBL*Δ*rbs*::P_{tac}-*glpX*Δ*gal*::P_{tac}-*tktA*Δ*tyrR*::*FRT*	Mohammadi Nargesi et al., 2018
4.4	0.17	glucose	Fed-batch	36	Pf_*papABC* & $aroG^{fbr}$	NST37 (DE3)Δ*pheLA*	Masuo et al. (2016)

effect on NPhe production (Fig. 5B–E). In support of this finding, no significant difference was observed in the aurF expression levels between strains harboring pZE12-aurF and pSAK-aurF (Fig. 5C–F). Alternatively focusing on the expression levels of Ec_pabB, strains with pSAK-Ptrc and pNE12-Ptrc showed high expression levels of Ec_pabB, which is consistent with the result of NPhe production (Fig. 5B–E). Indeed, the correlation between the transcription levels of Ec_pabB and NPhe was 0.73 (Fig. 5G), which is similar to the value shown in Fig. 4D. In contrast, the correlation between the transcription levels of aurF and NPhe was negligible (Fig. 5H). Furthermore, the ratio of Ec_pabB to aurF transcription levels in each strain almost corresponds to that of APhe to NPhe production: strains with low APhe accumulation tend to have lower Ec_pabB transcription levels than aurF ones (e.g., Fig. 5C pA_Ec_Pf, Fig. 5F pCD_Ec_Pf). In contrast, strains with high APhe accumulation showed opposite results (e.g., Fig. 5C pCD_Ec_Pf). These results indicate that the expression levels of APhe synthetic genes are more important than the *aurF* expression level for NPhe production from glucose.

3.5. Evaluation of alternative N-oxygenases: ObiL and NO16

As shown in Fig. 5E, pN_Ec_Pf produced 843 mg/L of NPhe, however, 276 mg/L of APhe remained accumulated. A previous study reported that ObiL and NO16 recognize both APhe and APP as substrates (Butler et al., 2023). Therefore, we assessed NPhe production by replacing AurF with ObiL or NO16. However, this substitution did not lead to an improvement in NPhe production titers (Fig. 6A and B). After 72 h of cultivation, PN-5 strain co-expressing EcpabAB-PfpapBC and ObiL produced 640 mg/L of NPhe, while the strain co-expressing EcpabAB-PfpapBC and NO16 produced 676 mg/L of NPhe. These titers were

comparable to those observed in the AurF expressing strain.

To further elucidate these findings, we determined the kinetic parameters of AurF, ObiL, and NO16 using purified enzymes (Tables 2 and 3, Fig. S2). The K_m value of ObiL for APP (0.10 mM) was approximately half that for APhe (0.19 mM), while the k_{cat} value for APP (3.2×10^{-2} s^{-1}) was six-fold higher than that for APhe (0.51×10^{-2} s^{-1}). A similar trend was observed for NO16, suggesting that both enzymes exhibit a preference for APP over APhe as a substrate. The catalytic efficiency (k_{cat}/K_m) for APP was determined to be 0.14 s^{-1} for AurF, 0.32 s^{-1} for ObiL, and 0.42 s^{-1} for NO16 (Table 3). Although ObiL and NO16 exhibited superior kinetic parameters compared to AurF, the NPhe titers obtained from glucose fermentation were comparable across all strains (Fig. 6A and B).

To further investigate APhe conversion efficiency, we evaluated NPhe production in strains expressing only ObiL or NO16 (i.e. without papABC expression) under conditions supplemented with about 1 g/L of APhe in M9Y medium (Fig. S3). Both strains successfully converted APhe into NPhe at levels superior to those observed with aurF-expressing strains (Fig. 1C), with molar conversion efficiencies of 0.83 ± 0.21 mol/mol (pZE12-aurF), 0.90 ± 0.01 mol/mol (pZE12-obiL), and 0.99 ± 0.07 mol/mol (pZE12-NO16). These findings suggest that the metabolic flux from APP to APhe, mediated by endogenous aminotransferases, is higher than both the conversion of APP to NPP by *N*-oxygenases and the reverse reaction (i.e. from APhe to APP), as summarized in Fig. 6C. It is supported by the fact that neither APP nor NPP detected during cultivation (Fig. 6A). In addition, a previous study reported that endogenous aminotransferases exhibit catalytic activities to oxo acids (e.g. phenylpyruvate) that are 10- to 100-fold higher than those toward their corresponding amino acids (e.g. phenylalanine) (Hayashi et al., 1993). Based on these results, a promising strategy for enhancing NPhe production from glucose would involve fine-tuning the metabolic fluxes governing the interconversion of APP and APhe, as well as the enhancing the flux from APP to NPP.

3.6. Batch fermentation in 4-nitrophenylalanine production

To enhance NPhe production, batch fermentation was performed in a 1-L bioreactor with the PN-5 strain harboring pNE12-Ptrc-EcpabAB-PfpapBC and pSAK-aurF. The culture conditions were similar to those described for APhe production, with some modifications, such as change in initial OD_{600} (see Materials and Methods for details). After 74 h of incubation, 2.22 g/L NPhe was produced, which was 2.6-fold higher than the titer obtained in the test tube culture (Fig. 7). The optimal pH for AurF activity is 5.5 (Chanco et al., 2014), suggesting that lower pH levels provide a more favorable environment for AurF-mediated reactions than the pH of 7 maintained in the bioreactor. However, adjusting the bioreactor cultivation pH to 6 did not result in improved NPhe production (data not shown). In the later stages of cultivation, the *E. coli* strain exhibited a marked decline in respiratory activity and glucose uptake capacity (data not shown). This finding is partially due to the toxicity of nitro compounds (Kovacic and Somanathan, 2014).

4. Conclusion

Here, we engineered *E. coli* strains capable of the biosynthesis of APhe and NPhe from glucose. Firstly, we demonstrated that the *N*-oxygenase AurF can be used for NPhe production. An optimal genetic configuration for APhe synthesis (*pabAB* from *E. coli* and *papBC* from *S. venezuelae*) was identified, and the engineered strain produced 2.52 g/L APhe in test tube cultivation and 22.5 g/L APhe in fed-batch cultivation. The co-expression of the *N*-oxygenase AurF along with the genes responsible for APhe production and the fine-tuning of the plasmid copy number allowed the production of 843 mg/L NPhe from glucose. After optimizing condition in batch cultivation, the NPhe titer reached 2.22 g/L.

Phenylalanine's role as a precursor for numerous compounds can enable the generation of nitrated phenylalanine derivatives via microbial fermentation. For example, phenylalanine is converted to cinnamic acid by phenylalanine ammonia lyase (Vargas-Tah and Gosset, 2015). Furthermore, styrene can be produced using cinnamic acid as a substrate (K. Lee et al., 2019; Liang et al., 2020.). 4-Nitrostyrene, wherein the 4-position of styrene is nitrated, has been utilized as a raw material for polymers (Gabr, 2007; Philippides et al., 1994). Phenylalanine is also a precursor of phenylacetaldehyde, phenylethanol, and flavonoids (S. P. Liu et al., 2015). Thus, our findings will aid in broadening the scope of nitrated compounds achievable through microbial production, extending beyond just the industrial synthesis of NPhe.

Table 2
Kinetic parameters of AurF, ObiL and NO16 to APhe.

Enzyme	K_m [mM]	k_{cat} [$\times 10^{-2}$ s^{-1}]	k_{cat}/K_m [mM^{-1} s^{-1}]
AurF	–	–	–
ObiL	0.19 ± 0.13	0.51 ± 0.09	0.027 ± 0.019
NO16	0.53 ± 0.19	1.3 ± 0.17	0.024 ± 0.0092

Table 3
Kinetic parameters of AurF, ObiL and NO16 to APP.

Enzyme	K_m [mM]	k_{cat} [$\times 10^{-2}$ s^{-1}]	k_{cat}/K_m [mM^{-1} s^{-1}]
AurF	0.15 ± 0.060	2.0 ± 0.23	0.14 ± 0.058
ObiL	0.10 ± 0.031	3.2 ± 0.32	0.32 ± 0.10
NO16	0.14 ± 0.13	5.8 ± 1.5	0.42 ± 0.41

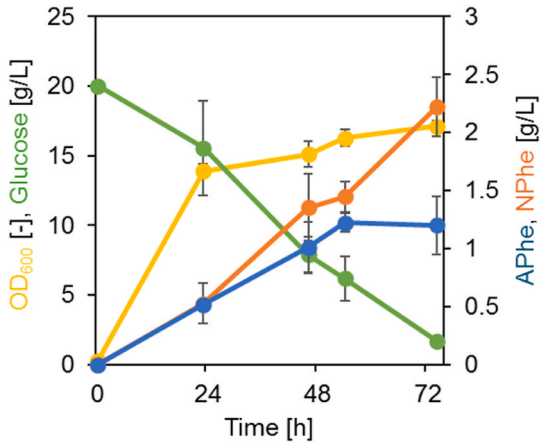

Fig. 7. Batch fermentation in NPhe production in a 1-L b**ioreactor.** APhe production, NPhe production, glucose concentration, and OD_{600} values are shown in blue, orange, green, and yellow, respectively. The data represent the means of three independent experiments with standard deviations. (For interpretation of the references to colour in this figure legend, the reader is referred to the Web version of this article.)

CRediT authorship contribution statement

Ayana Mori: Writing – original draft, Investigation, Conceptualization. **Yuuki Hirata:** Investigation. **Mayumi Kishida:** Investigation. **Daisuke Nonaka:** Investigation. **Akihiko Kondo:** Resources. **Yutaro Mori:** Writing – review & editing, Data curation. **Shuhei Noda:** Writing – review & editing, Investigation, Funding acquisition, Conceptualization. **Tsutomu Tanaka:** Writing – review & editing, Project administration, Investigation, Funding acquisition, Conceptualization.

Declaration of competing interests

The authors declare no financial or commercial conflict of interest.

Acknowledgements

This work was supported by the Japan Science and Technology Agency (JST), the Precursory Research for Embryonic Science and Technology (PRESTO) (Grant number JPMJPR22N9), Japan Society for the Promotion of Science (JSPS) Grants-in-Aid for Scientific Research (B) (Grant Number JP22H01885) and Grant-in-Aid for Scientific Research on Innovative Areas (Grant Number 23H04565) (to S.N.), and JSPS Grants-in-Aid for Scientific Research (B) (Grant Number JP22H01880) and the Sumitomo Foundation (to T.T.). The authors would like to thank Enago (www.enago.jp) for the English language review.

Appendix A. Supplementary data

Supplementary data to this article can be found online at https://doi.org/10.1016/j.ymben.2025.04.006.

Data availability

Data will be made available on request.

References

Barry, S.M., Kers, J.A., Johnson, E.G., Song, L., Aston, P.R., Patel, B., Krasnoff, S.B., Crane, B.R., Gibson, D.M., Loria, R., Challis, G.L., 2012. Cytochrome P450-catalyzed L-tryptophan nitration in thaxtomin phytotoxin biosynthesis. Nat. Chem. Biol. 8, 814–816. https://doi.org/10.1038/nchembio.1048.

Blanc, V., Gil, P., Bamas-Jacques, N., Lorenzon, S., Zagorec, M., Schleuniger, J., Bisch, D., Blanche, F., Debussche, L., Crouzet, J., Thibaut, D., 1997. Identification and analysis of genes from *Streptomyces pristinaespiralis* encoding enzymes involved in the biosynthesis of the 4-dimethylamino-l-phenylalanine precursor of pristinamycin I. Mol. Microbiol. 23, 191–202. https://doi.org/10.1046/J.1365-2958.1997.2031574.X.

Butler, N.D., Sen, S., Brown, L.B., Lin, M., Kunjapur, A.M., 2023. A platform for distributed production of synthetic nitrated proteins in live bacteria. Nat. Chem. Biol. 19, 911–920. https://doi.org/10.1038/s41589-023-01338-x.

Chanco, E., Choi, Y.S., Sun, N., Vu, M., Zhao, H., 2014. Characterization of the *N*-oxygenase AurF from *Streptomyces thioletus*. Bioorg. Med. Chem. 22, 5569–5577. https://doi.org/10.1016/j.bmc.2014.06.002.

Gabr, Y., 2007. Studies on the copolymerization of 4-aminostyrene with 4-nitro-and 2,4-dinitrostyrene scientific paper studies on the copolymerization of 4-aminostyrene with 4-nitro-and 2,4-dinitrostyrene. Acta Chim. Slov. 54, 818–824.

Gauba, V., Grünewald, J., Gorney, V., Deaton, L.M., Kang, M., Bursulaya, B., Ou, W., Lerner, R.A., Schmedt, C., Geierstanger, B.H., Schultz, P.G., Ramirez-Montagut, T., 2011. Loss of CD4 T-cell-dependent tolerance to proteins with modified amino acids. Proc. Natl. Acad. Sci. U.S.A 108, 12821–12826. https://doi.org/10.1073/pnas.1110042108.

Haiquan, Y., Yuxuan, X., Cui, Y., Wei, S., You, F., Xianzhong, C., 2019. Modular engineering of tyrosol production in *Escherichia coli*. J. Agric. Food Chem. 67 (14), 3900–3908. https://doi.org/10.1021/acs.jafc.9b00227.

Hayashi, H., Inoue, K., Nagata, T., Kuramitsu, S., Kagamiyama, H., 1993. *Escherichia coli* aromatic amino acid aminotransferase: characterization and comparison with aspartate aminotransferase. Biochemistry 32, 12229–12239. https://doi.org/10.1021/bi00096a036.

He, J., Hertweck, C., 2004. Biosynthetic origin of the rare nitroaryl moiety of the polyketide antibiotic aureothin: involvement of an unprecedented *N*-oxygenase. J. Am. Chem. Soc. 126, 3694–3695. https://doi.org/10.1021/ja039328t.

He, J., Magarvey, N., Piraee, M., Vining, L.C., 2001. The gene cluster for chloramphenicol biosynthesis in *Streptomyces venezuelae* ISP5230 includes novel shikimate pathway homologues and a monomodular non-ribosomal peptide synthetase gene. Microbiology (Read.) 147, 2817–2829. https://doi.org/10.1099/00221287-147-10-2817.

Hirayama, T., Kumar, A., Takada, K., Kaneko, T., 2020. Morphology-controlled self-assembly and synthesis of biopolyimide particles from 4-amino-l-phenylalanine. ACS Omega 5, 2187–2195. https://doi.org/10.1021/acsomega.9b03231.

Jiang, Y., Chen, B., Duan, C., Sun, B., Yang, J., Yang, S., 2015. Multigene editing in the *Escherichia coli* genome via the CRISPR-Cas9 system. Appl. Environ. Microbiol. 81, 2506–2514. https://doi.org/10.1128/AEM.04023-14.

Jobdevairakkam, C.N., Velladurai, H., 2009. Process of Making Optically Pure Melphalan, vol. 575, p. 385. U.S. Patent No. 8.

Jong-Won, L., Cong, T.T., 2022. Controlling selectivity of modular microbial biosynthesis of butyryl-CoA-derived designer esters. Metab. Eng. 69, 262–274. https://doi.org/10.1016/j.ymben.2021.12.001.

Kawasaki, Y., Aniruddha, N., Minakawa, H., Masuo, S., Kaneko, T., Takaya, N., 2018. Novel polycondensed biopolyamide generated from biomass-derived 4-aminohydrocinnamic acid. Appl. Microbiol. Biotechnol. 102, 631–639. https://doi.org/10.1007/s00253-017-8617-6.

Kovacic, P. Kovacic, Somanathan, R., 2014. Nitroaromatic compounds: environmental toxicity, carcinogenicity, mutagenicity, therapy and mechanism. J. Appl. Toxicol. 34 (8), 810–824. https://doi.org/10.1002/jat.2980.

Lee, J.K., Ang, E.L., Zhao, H., 2006. Probing the substrate specificity of aminopyrrolnitrin oxygenase (PrnD) by mutational analysis. J. Bacteriol. 188, 6179–6183. https://doi.org/10.1128/JB.00259-06.

Lee, K., Bang, H.B., Lee, Y.H., Jeong, K.J., 2019. Enhanced production of styrene by engineered *Escherichia coli* and in situ product recovery (ISPR) with an organic solvent. Microb. Cell Fact. 18, 79. https://doi.org/10.1186/s12934-019-1129-6.

Liang, L., Liu, R., Foster, K.E.O., AlakshChoudhury, C., Cook, S., Cameron, J.C., Srubar, W.V., Gill, R.T., 2020. Genome engineering of *E. coli* for improved styrene production. Metab. Eng. 57, 74–84. https://doi.org/10.1016/J.YMBEN.2019.09.007.

Liu, S.P., Zhang, L., Mao, J., Ding, Z.Y., Shi, G.Y., 2015. Metabolic engineering of *Escherichia coli* for the production of phenylpyruvate derivatives. Metab. Eng. 32, 55–65. https://doi.org/10.1016/J.YMBEN.2015.09.007.

Liu, X., Chen, S., Ma, Y., Xiao, W., 2020. Enantioseparation of 4-Nitrophenylalanine using (S)-SDP-metal complex as chiral extractant. Sep. Purif. Technol. 239, 116547. https://doi.org/10.1016/J.SEPPUR.2020.116547.

Lu, H., Chanco, E., Zhao, H., 2012. CmlI is an *N*-oxygenase in the biosynthesis of chloramphenicol. Tetrahedron 68, 7651–7654. https://doi.org/10.1016/j.tet.2012.06.036.

Martinez-Farina, C.F., Robertson, A.W., Yin, H., Monro, S., Mcfarland, S.A., Syvitski, R.T., Jakeman, D.L., 2015. Isolation and synthetic diversification of jadomycin 4-amino-l-phenylalanine. J. Nat. Prod. 78, 1208–1214. https://doi.org/10.1021/np5009398.

Masuo, S., Zhou, S., Kaneko, T., Takaya, N., 2016. Bacterial fermentation platform for producing artificial aromatic amines. Sci. Rep. 6, 25764. https://doi.org/10.1038/srep25764.

Mehl, R.A., Anderson, J.C., Santoro, S.W., Wang, L., Martin, A.B., King, D.S., Horn, D.M., Schultz, P.G., 2003. Generation of a bacterium with a 21 amino acid genetic code. J. Am. Chem. Soc. 125, 935–939. https://doi.org/10.1021/ja0284153.

Mohammadi Nargesi, B., Trachtmann, N., Sprenger, G.A., Youn, J.W., 2018. Production of *p*-amino-L-phenylalanine (L-PAPA) from glycerol by metabolic grafting of *Escherichia coli*. Microb. Cell Fact. 17, 149. https://doi.org/10.1186/s12934-018-0996-6.

Mori, A., Hirata, Y., Kishida, M., Mori, Y., Kondo, A., Noda, S., Tanaka, T., 2023. *p*-nitrobenzoate production from glucose by utilizing *p*-aminobenzoate *N*-oxygenase: AurF. Enzym. Microb. Technol. 171, 110321. https://doi.org/10.1016/j.enzmictec.2023.110321.

Nóbile, M.L., Stricker, A.M., Marchesano, L., Iribarren, A.M., Lewkowicz, E.S., 2021. N-oxygenation of amino compounds: early stages in its application to the biocatalyzed preparation of bioactive compounds. Biotechnol. Adv. 51, 107726. https://doi.org/10.1016/j.biotechadv.2021.107726.

Noda, S., Shirai, T., Oyama, S., Kondo, A., 2016. Metabolic design of a platform *Escherichia coli* strain producing various chorismate derivatives. Metab. Eng. 33, 119–129. https://doi.org/10.1016/j.ymben.2015.11.007.

Onuffer, J.J., Ton, B.T., Klement, I., Kirsch, J.F., 1995. The use of natural and unnatural amino acid substrates to define the substrate specificity differences of *Escherichia coli* aspartate and tyrosine aminotransferases. Protein Sci. 4, 1743–1749. https://doi.org/10.1002/PRO.5560040909.

Philippides, A., Budd, P.M., Price, C., Cuncliffe, A.V., 1994. The preparation and micellization behaviour of AB block copolymers of styrene and 4-nitrostyrene. Polymer 35, 1759–1763. https://doi.org/10.1016/0032-3861(94)90852-4.

Siddharth, S. Patel, Dhaval, B. Patel, Hitesh, D. Patel, 2021. Synthetic protocols for aromatic nitration: a review. ChemistrySelect 6, 1337–1356. https://doi.org/10.1002/slct.202004695.

Tateyama, S., Masuo, S., Suvannasara, P., Oka, Y., Miyazato, A., Yasaki, K., Teerawatananond, T., Muangsin, N., Zhou, S., Kawasaki, Y., Zhu, L., Zhou, Z., Takaya, N., Kaneko, T., 2016. Ultrastrong, transparent polytruxillamides derived from microbial photodimers. Macromolecules 49, 3336–3342. https://doi.org/10.1021/acs.macromol.6b00220.

Tomita, H., Katsuyama, Y., Minami, H., Ohnishi, Y., 2017. Identification and characterization of a bacterial cytochrome P450 monooxygenase catalyzing the 3-nitration of tyrosine in rufomycin biosynthesis. J. Biol. Chem. 292, 15859–15869. https://doi.org/10.1074/jbc.M117.791269.

Tsao, M.L., Summerer, D., Ryu, Y., Schultz, P.G., 2006. The genetic incorporation of a distance probe into proteins in *Escherichia coli*. J. Am. Chem. Soc. 128, 4572–4573. https://doi.org/10.1021/ja058262u.

Vargas-Tah, A., Gosset, G., 2015. Production of cinnamic and *p*-hydroxycinnamic acids in engineered microbes. Front. Bioeng. Biotechnol. 3, 116. https://doi.org/10.3389/fbioe.2015.00116.